Downloaded from jnis.bmj.com on February 27, 2012 - Published by group.bmj.com

ORIGINAL RESEARCH

Patient based computational fluid dynamic characterization of carotid bifurcation stenosis before and after endovascular revascularization

Clemens M Schirmer,[1] Adel M Malek[2]

[1]Division of Neurosurgery, Baystate Medical Center, Springfield, Massachusetts, USA
[2]Department of Neurosurgery, Tufts Medical Center, Boston, Massachusetts, USA

Correspondence to
Dr A M Malek, Department of Neurosurgery, Tufts Medical Center, 800 Washington St, No 178, Boston, MA 02111, USA; amalek@tuftsmedicalcenter.org

Received 3 May 2011
Accepted 3 September 2011

ABSTRACT

Introduction Hemodynamic forces play a critical role in determining the molecular phenotype of the endothelial cell and in influencing vascular remodeling. A lesion based computational fluid dynamic (CFD) modeling approach is presented to understand the complex spatial and temporal hemodynamic changes that prevail in carotid stenosis (CS) in patients with critical CS undergoing carotid artery stenting (CAS).

Methods High resolution three-dimensional rotational angiography volumetric datasets were acquired before and after treatment in eight patients, segmented and used to generate a high quality structured hexahedral computational mesh with boundary layer refinement. CFD analysis was carried out using a time dependent laminar flow model implementing non-Newtonian realistic blood viscosity for blood, and used to compute wall shear stress (WSS) and its gradient (WSSG).

Results CAS restored fully or near laminar flow in all cases in our series. In addition, WSS was found to decrease in the stented region in all cases, reduced to near normal levels of 34 ± 14 dyn/cm^2 with significant blunting of the extreme pretreatment WSSG to levels lower than 1000 dyn/cm^3.

Conclusions In this series of patients with symptomatic CS, CFD simulation enabled estimation of the hemodynamic effect of CAS, leading to reversal of abnormal flow patterns and wall shear forces around the arterial stenosis, with normalization of flow laminarity and wall shear spatiotempotal patterns known to be associated with adverse endothelial cell function.

INTRODUCTION

The diagnosis of symptomatic carotid artery stenosis (CS) is made based on a combination of history, clinical examination and imaging information derived from CT, MR tomographic, ultrasonographic Doppler information and angiographic images. Despite the rapid advancement of non-invasive imaging modalities, biplane and rotational digital subtraction angiography still provide unsurpassed anatomic resolution of the endoluminal aspect of CS. Evaluation of angiographic images remains, however, limited to the measurement of the geometric degree of stenosis, leaving the evaluation of a stenosis to the experience of the treating physician. Computational fluid dynamic (CFD) methods can offer an additional important layer of functional information to enrich and complement the anatomical information.

Most biomechanical studies of carotid artery bifurcations assume conditions such as steady flow,[1] pulsatile flow,[2] compliant materials[3] and certain geometric effects, including changing bifurcation angles[2 4] and wall curvature.[5] These studies have centered their attention on defining the pattern of blood flow within the stenotic vessel, and have lacked adequate resolution to estimate wall shear stress (WSS).[6 7] We sought to characterize the spectrum of wall shear forces in space and time within high resolution patient CS geometries using CFD analysis with a fine computational mesh and a realistic non-Newtonian Carreau–Yasuda formulation of blood viscosity. We examine here cervical carotid lesions before and after carotid angioplasty and carotid artery stenting (CAS) to characterize the nature of the pathophysiological hemodynamic milieu and to evaluate the effect of endovascular treatment in restoring the micromechanical environment at the vessel wall.

PATIENTS AND METHODS

Eight patients (two women, median age 76 years) with symptomatic CS recalcitrant to medical therapy were selected to undergo CAS using self-expanding stents. Five lesions were located on the left side (63%). The patients underwent catheter based digital subtraction cerebral angiography in biplane and three-dimensional rotational modes.[8] Median degree of stenosis by ultrasonographic Doppler examinations performed in seven of eight patients was 95% and median angiographic stenosis was 88% by NASCET criteria.[9] All patients underwent subsequent CAS with deployment of a nitinol shape memory alloy self-expanding stent (Precise Stent, Cordis-Johnson and Johnson, New Jersey, USA) followed by repeat angiographic image acquisition (figure 1).

A detailed description of the computational methods has been previously described.[10 11] Briefly, the three-dimensional volumetric datasets, reconstructed from rotational angiograms, were segmented and used to generate hybrid, predominantly hexahedral meshes with refinement zones over the area of the carotid bifurcation and the internal carotid. Numerical computations were carried out using Fluent (V.6.2.16, Fluent Inc, Lebanon, New Hampshire, USA)[12] on a cluster of parallel computers. A transient laminar flow model using a Carreau non-Newtonian formulation of the viscous properties of blood,[10 11 13 14] non-slip and non-penetration constraints at the wall were

Downloaded from jnis.bmj.com on February 27, 2012 - Published by group.bmj.com

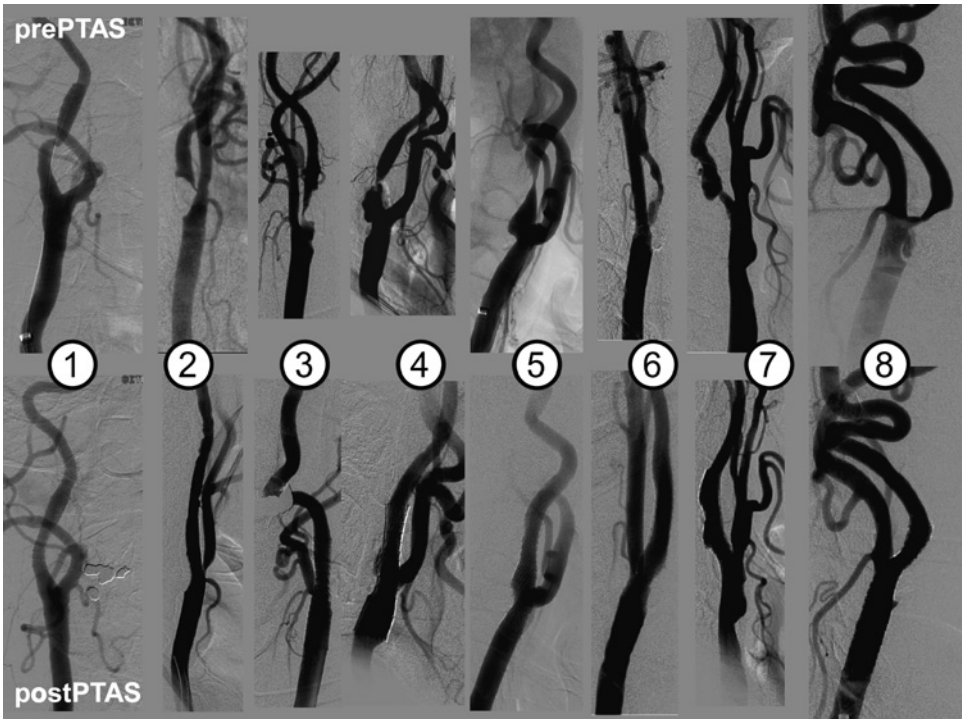


Figure 1 Single plane angiographic projections of the stenotic lesions of the carotid before (upper panel) and after (lower panel) percutaneous carotid artery angioplasty and stenting. (PTAS).

assumed for the simulations. Pulsatile CFD was performed for three cardiac cycles[10] with a 500 timestep pulsatile velocity waveform that was derived from waveforms previously described in healthy human subjects by Ford *et al*[15] prescribed at the common carotid inlet. The Reynolds number of the mean flow of 6.0 ml/s in the common carotid artery was 361 and the Womersley number[16] describing the waveform was 4.9.

The computational approach used in the current study has been previously validated[10 11 17] using published experimental data.[10 18] Lack of dependence on grid density, inlet boundary condition and periodicity were established as described previously[11] using mesh sizes ranging from 35 000 to 1 200 000 cells for a given carotid lesion. No significant difference was observed beyond a mesh of 201×10^3 elements in velocity and shear stress distributions. We chose a target mesh size of 900 000 elements to optimize the accuracy of gradient derivatives and computational time.

Post-processing was performed using Ensight software (V.8, Computational Engineering International, Apex, North Carolina, USA). The oscillatory shear index (OSI), a measure for areas with shear vectors that change direction over the course of the pulse cycle, was calculated as[19]

$$OSI = 1/2\left(1 - \frac{\left|\int_0^T \overrightarrow{\tau_w} dt\right|}{\int_0^T |\overrightarrow{\tau_w}| dt}\right)$$

where τ_w is the instantaneous WSS vector and T denotes the length of the pulse cycle. We also defined the dynamic angular shear deviation (DASD) calculated as:

$$\alpha_1 = \arctan\left(\overrightarrow{\tau_x}/\overrightarrow{\tau_y}\right), \alpha_2 = \arctan\left(\overrightarrow{\tau_x}/\overrightarrow{\tau_z}\right), \alpha_3 = \arctan\left(\overrightarrow{\tau_y}/\overrightarrow{\tau_z}\right)$$

$$DASD = \frac{1}{T}\int_0^T \left\| \sum_{i=1}^{3} \alpha_i - \frac{1}{T}\int_0^T \sum_{i=1}^{3} \alpha_i dt \right\| dt$$

where $\overrightarrow{\tau_{\{x,y,z\}}}$ is the instantaneous WSS vector component in x, y and z direction and T denotes the length of the pulse cycle. DASD gives a measure of the angular variation of the instantaneous WSS vector over time with respect to the temporal average WSS vector, taken over the entire pulse cycle.

Statistical analysis of mean values was performed using Student's t tests and statistical significance was assumed for $p<0.05$ (SAS, Cary, North Carolina, USA).

RESULTS

CS results in a complex flow pattern inside the stenosis and downstream with associated intricate and heterogeneous changes of the wall shear magnitude and direction in space and time. Analysis of the reconstructed carotid arteries of the patients in this study following CAS predicted that intervention alleviated the increased WSS magnitude in the region of the stenosis. In analogy to the analysis of the stenotic geometries, we defined two regions of interest (see insert figure 2C): the distal common carotid artery (CCA) and the area of the wall covered by the stent. Values were averaged spatially and temporally and the mean of all cases in this study was taken (figure 2C). The average WSS magnitude at the level of the stent was 34 ± 14 dyn/cm^2, not significantly increased from 25 ± 8 dyn/cm^2 in the CCA segment upstream ($p=0.14$). WSS magnitude in the upstream CCA segments in the carotid reconstructions after CAS was not different compared with 23 ± 11 dyn/cm^2 in the healthy CCA segment of the carotid reconstructions with CS ($p=0.78$). WSS magnitude distribution, time averaged over the cardiac cycle, was predicted to have normalized WSS (compare figure 2A and figure 4A). WSS vector direction in the post-stenotic dilatation in the stenotic geometries of the cases before CAS was skewed and even retrograde in areas that migrate over time. CAS restored alignment of the WSS in the direction of mean flow (figure 4B). Although the direction of WSS forces after CAS remains because of parent vessel tortuosity, the areas of retrograde WSS vectors are much smaller and appear in four cases, mostly in areas of size mismatch (case Nos 4, 5 and 7, circles in figure 4B). The spatial WSS gradient (WSSG) magnitude after CAS is markedly reduced and only very small areas exhibit WSSG values exceeding 1000 dyn/cm^3 (figure 4C).

Downloaded from jnis.bmj.com on February 27, 2012 - Published by group.bmj.com

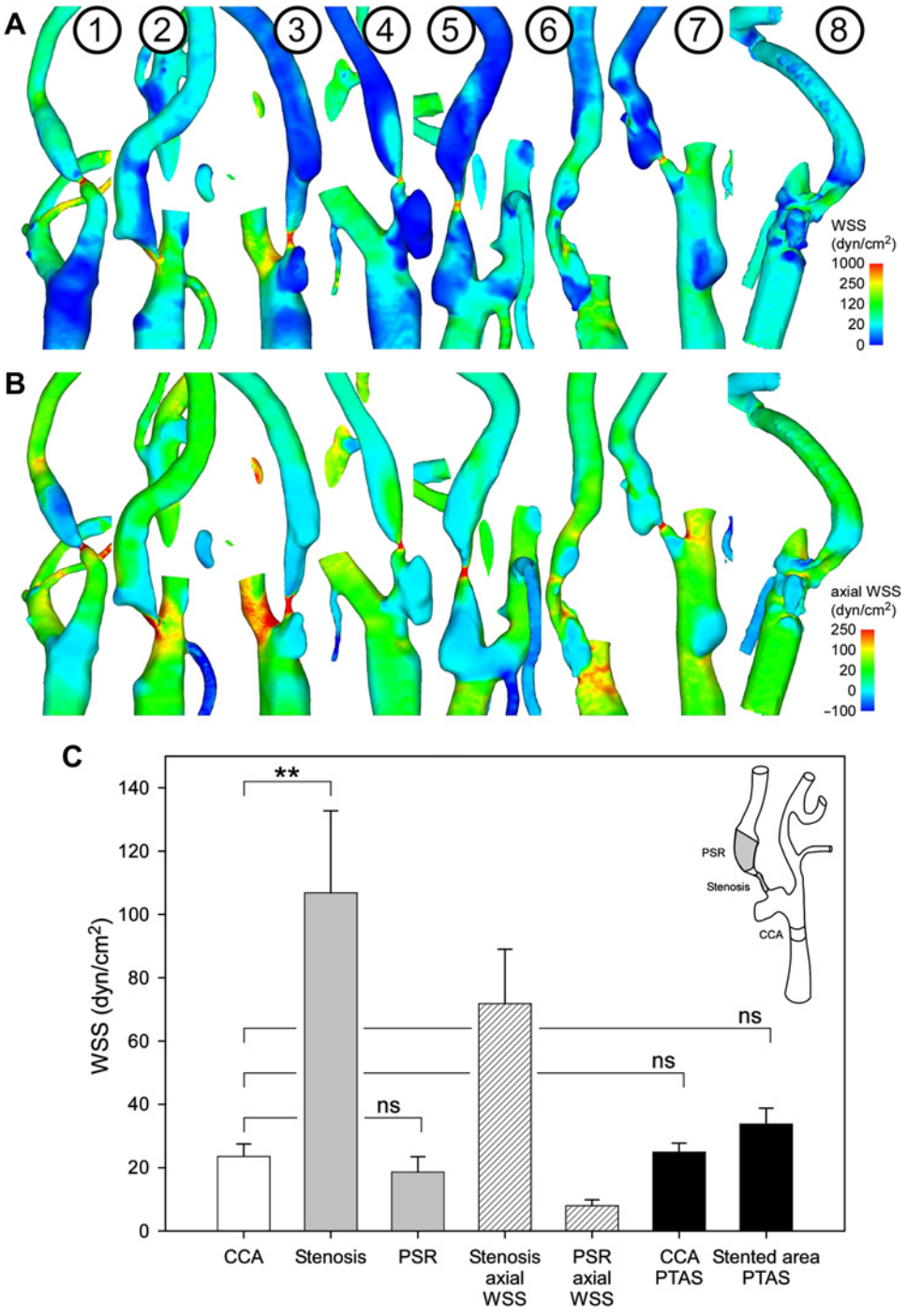


Figure 2 Contour plots of the wall shear stress (WSS) magnitude (A) and the axial WSS component (B) averaged over the cardiac cycle. (C) Bar graph showing time averaged and spatially averaged mean magnitudes of the WSS and directional magnitudes of the antegrade WSS in the distal common carotid artery (CCA), at the stenosis, at the expansion of the post-stenotic region (PSR), the CCA in the vessel after carotid artery stenting (PTAS) and the stented area after PTAS. Values are mean±SD; the insert shows the schematic position of the regions of interest.

OSI[19] is a known normalized index that identifies regions undergoing relatively increased changes of WSS direction compared with the temporal average. Figure 3A depicts the spectrum of OSI distribution for all cases, with regions of increased OSI corresponding to regions of rapid WSS directional changes (compare with figure 4).

We defined the DASD as a parameter that expresses the degree of temporal changes of the angle of the WSS direction compared with the temporal average, giving a measure of how well the average WSS vector aligns with the temporal average WSS vector over the course of the pulse cycle. This accounts for the sensitivity of endothelial cells to directional changes to complement the changes in magnitude that are summarized by the OSI. Contour plots of the predicted DASD are shown for all cases (figure 3C). Areas of increased DASD appear in the post-stenotic region in case Nos 1–5 and 7. In the cases of the elongated stenosis in case Nos 6 and 8, the DASD appears to be increased in the initial segment of the stenosis (circles in figure 3C).

DISCUSSION

In this study, we examined the changes in flow patterns and the distribution of wall shear forces and their spatiotemporal derivatives in patient based models of the carotid bifurcation in patients before and after CAS.

Modeling the effects of CAS

CAS not only restored fully or near laminar flow in all cases in our series, we also found that, in all cases, WSS in the stented region was reduced to 34±14 dyn/cm^2 with little or no significant

Downloaded from jnis.bmj.com on February 27, 2012 - Published by group.bmj.com

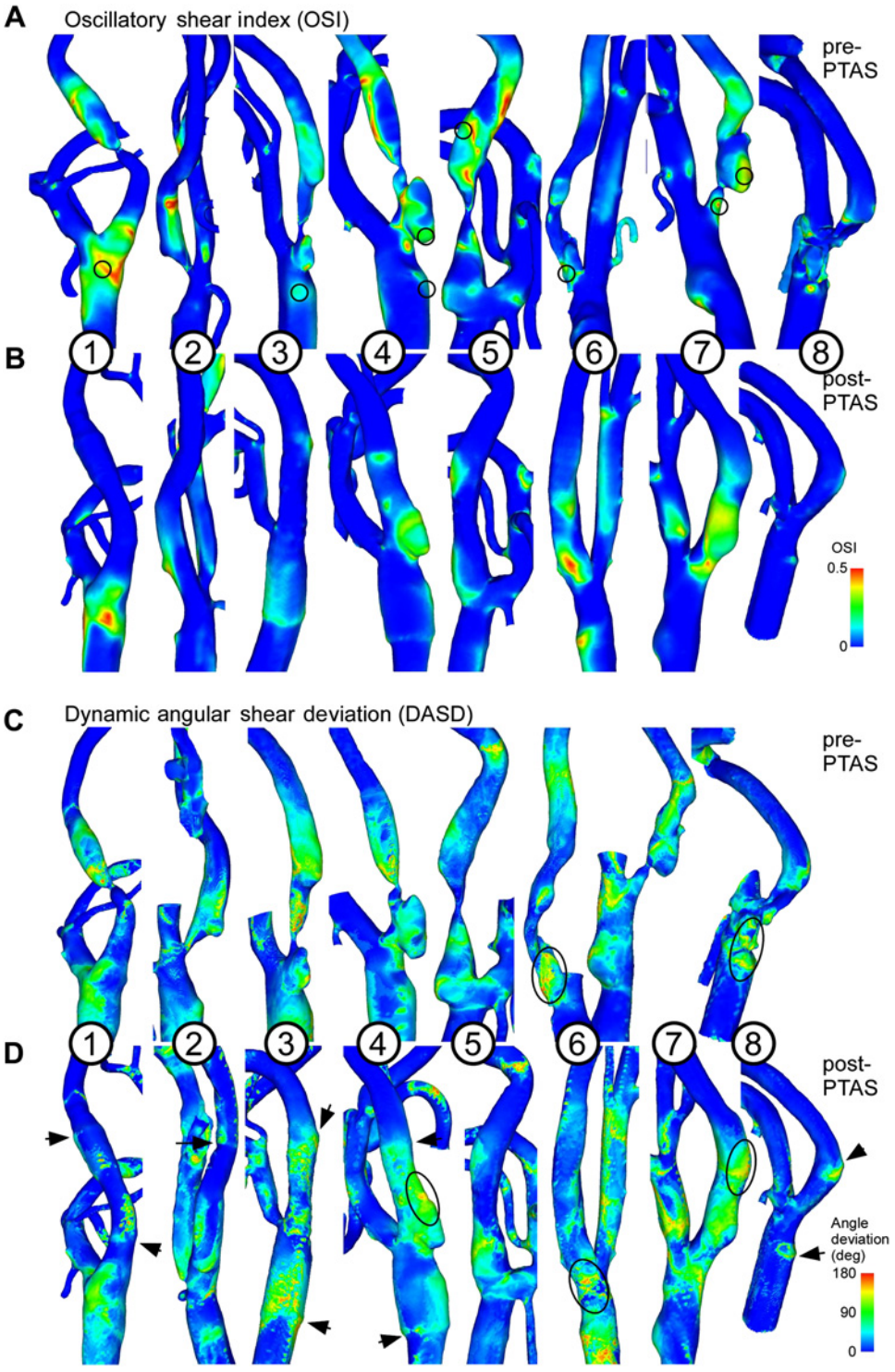


Figure 3 Oscillatory shear index (OSI) contour plots in all lesions prior to (A) and following (B) carotid artery stenting (PTAS), and dynamic angular shear deviation (DASD) before (C) and after (D) PTAS. External carotid artery branches were cropped when overlaying the internal carotid artery.

WSSG in excess of 1000 dyn/cm^3 (figure 4). Regions of elevated OSI have been associated in human aortas with the occurrence of sudanophilic lesions which are suggested to be precursors of atherosclerosis.[20] In agreement with our data, regions of high OSI colocalized with low values of time averaged shear (figures 2A and 3A). CAS caused the majority of the originally identified regions of elevated OSI to disappear (figure 3B) and to be replaced by smaller and less prominent regions of high OSI colocalized with the edges of the stented segment of the vessel.

We introduced DASD as a parameter to estimate the magnitude of the temporal variation of the WSS vector direction against its temporal mean over the entire cycle. Although this parameter has not been investigated in an experimental setup with respect to its correlation with the endothelial response to different DASD values, it yields a map of areas that are predicted to undergo large directional changes in the shear stress vector. Following CAS, regions of increased DASD were noted in regions near the proximal and distal ends of the stent and in areas of residual stenosis (figure 3C,D). Future spatial analysis of stent restenosis and its correlation with OSI and DASD will be needed to determine their relative predictive value.

Downloaded from jnis.bmj.com on February 27, 2012 - Published by group.bmj.com

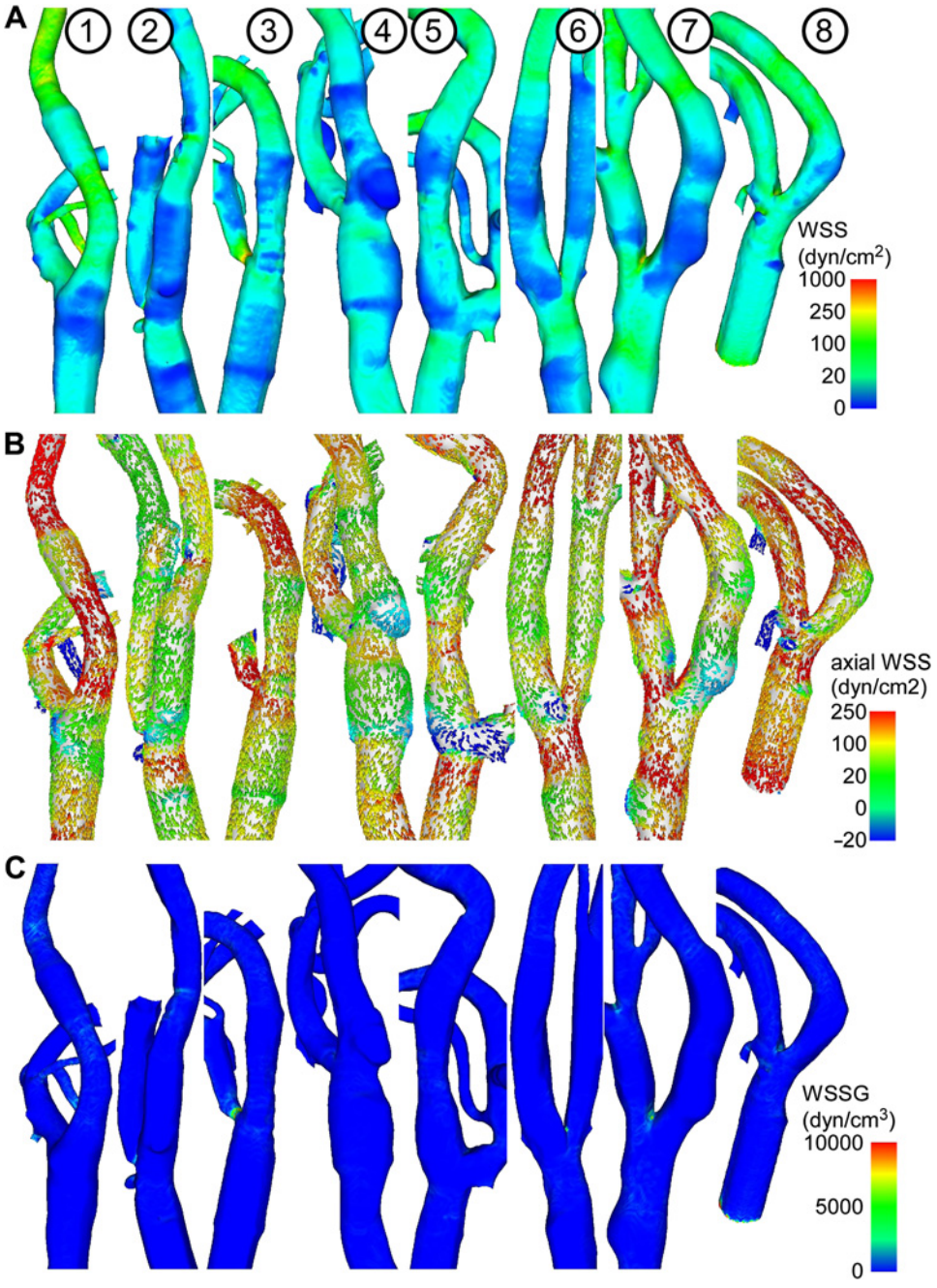


Figure 4 Contour plots of the wall shear stress (WSS) magnitude averaged over the cardiac cycle (A) and the WSS vectors colored by the axial WSS gradient (WSSG) component during peak systole (B) after carotid artery stenting. (C) Contour plots of the WSSG magnitude averaged over the cardiac cycle.

Biological implications

One may argue that the insight derived from the results of this study into the biology of vascular cells and the development of atherosclerosis is limited. Nonetheless, the intent of the current study was not to describe a novel biological response but rather to obtain the most realistic estimates of the blood flow characteristics as is currently possible using a state of the art CFD technique. The knowledge gleaned from the current modeling approach provides a starting point for the study of the biological response of platelets and other vascular cells to the hemodynamic conditions encountered in the study. Modeling and biological experiments complement each other: the predictions of the ranges and dynamics of the shear rates in realistic patient based lesions in this study can be used to set the parameters for experimental setups.

It is difficult to know what shear rate and stress to subject platelets and vascular cells in order to mimic the in vivo environment without first obtaining a realistic model of the hemodynamic conditions, which cannot be directly measured with a sufficiently high spatial/temporal resolution in the patient. Similarly, the results from the current study help better put in context the biological results from mechano-transduction experiments on vascular cells obtained in vitro with respect to actual carotid stenotic lesions. Animal models may be a compromise but to date it remains unclear how well such models, most of which are based on high cholesterol diets, reflect realistic patient based lesions.

It is hoped that the results from the current study will enable the setup of improved experiments to better mimic the hemodynamic microenvironment of the carotid atherosclerotic lesion in its temporal and spatial complexity, in the hope of achieving improved identification of the biological responses likely to occur within these morphologically complex lesions.

Downloaded from jnis.bmj.com on February 27, 2012 - Published by group.bmj.com

Limitations of this study

The approach undertaken in the current study focused on modeling the hemodynamic conditions within the flow channel and the shear stress generated by the flow on the vessel wall. As outlined above, these forces result in a multitude of effects on the morphology and function of the cells of the vessel wall and the formed elements within blood. Our type of modeling approaches does not incorporate a feedback component. Rather, it is a reductionist approach that does not account for the complex multicellular autocrine and paracrine interactions among the various vessel wall cells and components. Accordingly, it is a snapshot in time, well after carotid stenosis has already progressed to a symptomatic lesion.

Our current modeling technique assumes a rigid wall[21] and disregard for plaque composition and heterogeneity; it is accordingly not well suited at evaluating the tensile stresses within vulnerable plaque, such as recently demonstrated by Li *et al*[22] to play an important role in plaque rupture and distal embolization. Analysis of the viscoelastic and probably non-uniform spatial properties of an atherosclerotic vessel wall would require knowledge not only of lesion geometry but also a definition of the components of its heterogeneous material composition and their material properties. Such an analysis would require the use of fluid structure interaction (FSI) techniques that offer a solution by taking the deformation of the computational mesh by the prevailing pressure field iteratively into account, resulting in considerably larger computational requirements. Previous FSI analysis of a vessel stenosis utilized a smaller grid size of 32 000 cells[23] (compared with ~900 000 cells in this study) which would be insufficient to study the details of the flow in the post-stenotic region. Nonetheless, it remains unclear if the assumption of an elastic wall would fundamentally alter the basic premise of our findings; a recent study of wall stress in a model of an abdominal aortic aneurysm showed minimal difference (of the order of 1%) between the rigid and elastic wall (FSI) models.[24]

Ignoring the viscoelastic properties, the non-Newtonian properties of blood were captured here using the Carreau–Yasuda model which captures the shear thinning behavior of blood as its dominant component.[25] In another report on the model of a 25%, 50% and 75% stenosis the peak antegrade WSS measured at peak systolic flow on the wall at the throat of the stenosis was increased by 59%, 5% and 6%, respectively, while no shifts in location of the reversal points of WSS and WSSG were observed when comparing the shear thinning Carreau model with a constant viscosity Newtonian model.[10] Assuming a Newtonian fluid resulted in underestimation of both WSS and its gradient, consistent with previous studies showing non-Newtonian flows to exhibit a more blunt velocity profile with higher resulting wall forces.[26]

The time averaged maximum Reynolds number inside the simulated volume is below the limit usually assumed for the occurrence of turbulent flow, justifying our use of a laminar flow model. Models that account explicitly for the development of turbulent flow regimens are nevertheless of great interest, and other groups have used Reynolds averaged techniques (such as the k-ε and k-ω model)[27 28] that can model turbulence to study idealized axisymmetric stenoses. These efforts have met with poor agreement of basic velocity and shear predictions with experimental results. More recently, direct numerical simulation has been employed to achieve the same goal with better results.[29]

Modeling vessel geometry following CAS using our current approach does not explicitly reproduce the geometry of the stent struts. While it would certainly be desirable to examine the CFD conditions immediately after CAS and the changes caused by the stent struts, and their potential disruptive effect on the shear field on the wall, the imaging modalities currently in use in clinical practice do not provide the sufficient high resolution needed to resolve the details of the stent geometry inside the vessel.

The findings from this study are patient specific and should not be simply generalized to a different patient population because of the inherent heterogeneous features of carotid stenosis. The current study focused on the possible effects of hemodynamic condition within carotid artery stenosis on forces exerted on the cell situated at the wall.

CONCLUSION

In this series of patients with symptomatic CS that underwent CAS, we examined the abnormal flow pattern and wall shear forces around the stenotic area estimated by CFD simulation. These changes vary over the pulse cycle and give rise to temporal and spatial WSSGs, forming narrow bands of antegrade and retrograde WSSG next to areas of increased WSS. The magnitude and location of these regions of increased WSSG undergo cyclic changes over the cardiac cycle, exposing endothelium in these areas to repetitive changes in direction and magnitude of the WSS and WSSG, with elevated OSI. CAS changes the local flow environment and leads to normalization of flow and wall parameters related to adverse endothelial cell function. We hope that these results will provide data to guide further experimental studies and understanding of the hemodynamic component of the mutifactorial driving forces behind the progression of carotid disease and the development of appropriate treatment strategies.

Competing interests None.

Contributors CMS and AMM contributed equally to the manuscript.

Provenance and peer review Not commissioned; externally peer reviewed.

REFERENCES

1. **Bharadvaj BK,** Mabon RF, Giddens DP. Steady flow in a model of the human carotid bifurcation. Part II—laser-Doppler anemometer measurements. *J Biomech* 1982;**15**:363–78.
2. **Wells DR,** Archie JP Jr, Kleinstreuer C. Effect of carotid artery geometry on the magnitude and distribution of wall shear stress gradients. *J Vasc Surg* 1996;**23**:667–78.
3. **Perktold K,** Rappitsch G. Computer simulation of local blood flow and vessel mechanics in a compliant carotid artery bifurcation model. *J Biomech* 1995;**28**:845–56.
4. **Wong PK,** Johnston KW, Ethier CR, *et al*. Computer simulation of blood flow patterns in arteries of various geometries. *J Vasc Surg* 1991;**14**:658–67.
5. **Kleinstreuer C,** Hyun S, Buchanan JR Jr, *et al*. Hemodynamic parameters and early intimal thickening in branching blood vessels. *Crit Rev Biomed Eng* 2001;**29**:1–64.
6. **Botnar R,** Rappitsch G, Scheidegger MB, *et al*. Hemodynamics in the carotid artery bifurcation: a comparison between numerical simulations and in vitro MRI measurements. *J Biomech* 2000;**33**:137–44.
7. **Kohler U,** Marshall I, Robertson MB, *et al*. MRI measurement of wall shear stress vectors in bifurcation models and comparison with CFD predictions. *J Magn Reson Imaging* 2001;**14**:563–73.
8. **Hoit DA,** Malek AM. Three-dimensional rotational angiographic detection of in-stent stenosis in wide-necked aneurysms treated with a self-expanding intracranial stent. *Neurosurgery* 2005;**57**:1228–36.
9. **Anon;** North American Symptomatic Carotid Endarterectomy Trial. Methods, patient characteristics, and progress. *Stroke* 1991;**22**:711–20.
10. **Schirmer CM,** Malek AM. Wall shear stress gradient analysis within an idealized stenosis using non-Newtonian flow. *Neurosurgery* 2007;**61**:853–64.
11. **Schirmer CM,** Malek AM. Prediction of complex flow patterns in intracranial atherosclerotic disease using computational fluid dynamics. *Neurosurgery* 2007;**61**:842–52.
12. **Fluent.** *FLUENT 6.2 User's Guide*. Lebanon, NH: Fluent Inc, 2005.
13. **Thurston GB.** Frequency and shear rate dependence of viscoelasticity of human blood. *Biorheology* 1973;**10**:375–81.
14. **Thurston GB.** Rheological parameters for the viscosity viscoelasticity and thixotropy of blood. *Biorheology* 1979;**16**:149–62.

Downloaded from jnis.bmj.com on February 27, 2012 - Published by group.bmj.com

15. **Holdsworth DW,** Norley CJ, Frayne R, *et al*. Characterization of common carotid artery blood-flow waveforms in normal human subjects. *Physiol Meas* 1999;**20**:219—40.
16. **Womersley JR.** Method for the calculation of velocity, rate of flow and viscous drag in arteries when the pressure gradient is known. *J Physiol* 1955;**127**:553—63.
17. **Schirmer CM,** Malek AM. Estimation of wall shear stress dynamic fluctuations in intracranial atherosclerotic lesions using computational fluid dynamics. *Neurosurgery* 2008;**63**:326—34.
18. **Ahmed SA,** Giddens DP. Pulsatile poststenotic flow studies with laser Doppler anemometry. *J Biomech* 1984;**17**:695—705.
19. **Hyun S,** Kleinstreuer C, Longest PW, *et al*. Particle-hemodynamics simulations and design options for surgical reconstruction of diseased carotid artery bifurcations. *J Biomech Eng* 2004;**126**:188—95.
20. **Cornhill JF,** Herderick EE, Stary HC. Topography of human aortic sudanophilic lesions. *Monogr Atheroscler* 1990;**15**:13—19.
21. **Liu Y,** Lai Y, Nagaraj A, *et al*. Pulsatile flow simulation in arterial vascular segments with intravascular ultrasound images. *Med Eng Phys* 2001;**23**:583—95.
22. **Li ZY,** Howarth SP, Tang T, *et al*. How critical is fibrous cap thickness to carotid plaque stability? A flow-plaque interaction model. *Stroke* 2006;**37**:1195—9.
23. **Tang D,** Yang C, Kobayashi S, *et al*. Steady flow and wall compression in stenotic arteries: a three-dimensional thick-wall model with fluid-wall interactions. *J Biomech Eng* 2001;**123**:548—57.
24. **Leung JH,** Wright AR, Cheshire N, *et al*. Fluid structure interaction of patient specific abdominal aortic aneurysms: a comparison with solid stress models. *Biomed Eng Online* 2006;**5**:33.
25. **Gijsen FJ,** van de Vosse FN, Janssen JD. The influence of the non-Newtonian properties of blood on the flow in large arteries: steady flow in a carotid bifurcation model. *J Biomech* 1999;**32**:601—8.
26. **Buchanan JR Jr,** Kleinstreuer C, Comer JK. Rheological effects on pulsatile hemodynamics in a stenosed tube. *Comput Fluid* 2000;**29**:695—724.
27. **Varghese SS,** Frankel SH. Numerical modeling of pulsatile turbulent flow in stenotic vessels. *J Biomech Eng* 2003;**125**:445—60.
28. **Ryval J,** Straatman AG, Steinman DA. Two-equation turbulence modeling of pulsatile flow in a stenosed tube. *J Biomech Eng* 2004;**126**:625—35.
29. **Beratlis N,** Balaras E, Parvinian B, *et al*. A numerical and experimental investigation of transitional pulsatile flow in a stenosed channel. *J Biomech Eng* 2005;**127**:1147—57.

Downloaded from jnis.bmj.com on February 27, 2012 - Published by group.bmj.com



Patient based computational fluid dynamic characterization of carotid bifurcation stenosis before and after endovascular revascularization

Clemens M Schirmer and Adel M Malek

J NeuroIntervent Surg published online October 28, 2011
doi: 10.1136/neurintsurg-2011-010070

Updated information and services can be found at:
http://jnis.bmj.com/content/early/2011/10/28/neurintsurg-2011-010070.full.html

These include:

References This article cites 28 articles, 3 of which can be accessed free at:
http://jnis.bmj.com/content/early/2011/10/28/neurintsurg-2011-010070.full.html#ref-list-1

P<P Published online October 28, 2011 in advance of the print journal.

Email alerting service Receive free email alerts when new articles cite this article. Sign up in the box at the top right corner of the online article.

Topic Collections Articles on similar topics can be found in the following collections

Basic science (12 articles)

Notes

Advance online articles have been peer reviewed, accepted for publication, edited and typeset, but have not not yet appeared in the paper journal. Advance online articles are citable and establish publication priority; they are indexed by PubMed from initial publication. Citations to Advance online articles must include the digital object identifier (DOIs) and date of initial publication.

To request permissions go to:
http://group.bmj.com/group/rights-licensing/permissions

To order reprints go to:
http://journals.bmj.com/cgi/reprintform

To subscribe to BMJ go to:
http://group.bmj.com/subscribe/